Article:
Pratama, Y, Simone, E orcid.org/0000-0003-4000-2222 and Rappolt, M orcid.org/0000-0001-9942-3035 (2021) The Unique Crystallization Behavior of Buffalo Milk Fat. Crystal Growth & Design, 21 (4). pp. 2113-2127. ISSN 1528-7483

https://doi.org/10.1021/acs.cgd.0c01543

Supplementary Information

The Unique Crystallisation Behaviour of Buffalo Milk Fat

Yoga Pratama[1,2], Elena Simone[1] and Michael Rappolt*[1]

[1]School of Food Science and Nutrition, University of Leeds, Leeds LS2 9JT, U.K.

[2]Department of Food Technology, Faculty of Animal and Agricultural Sciences, Diponegoro University, Jl. Prof. Soedarto Tembalang Semarang 50275, Indonesia

List of Figures

List of Tables

*Corresponding author: e-mail m.rappolt@leeds.ac.uk

1. Mass Spectroscopy Data

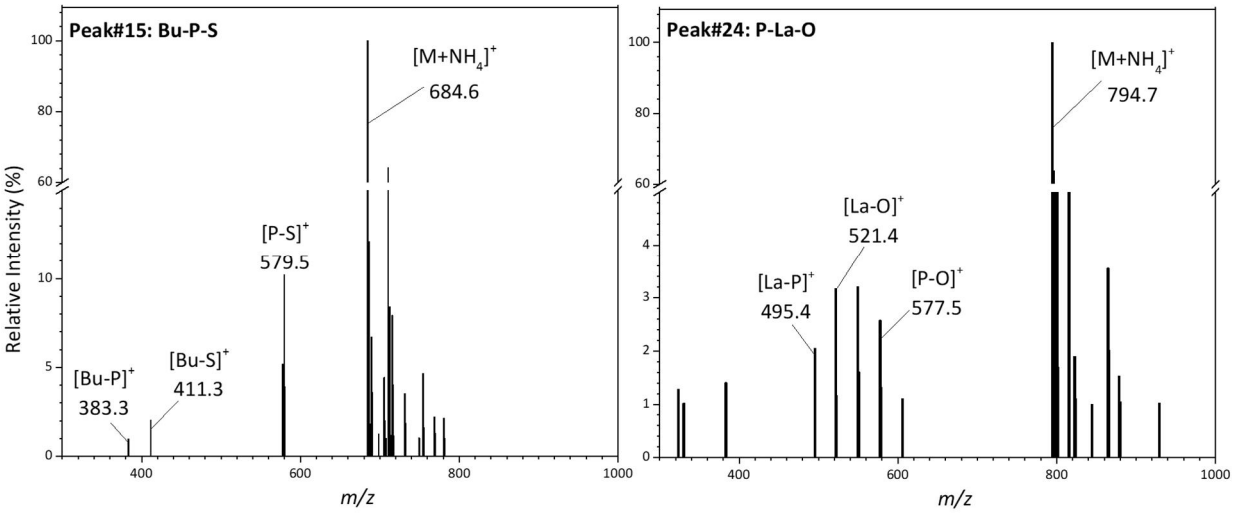

Figure S1. Identification of selected peaks from Figure 1 (peak number is indicated in the figure) based on its mass spectra. $[M+NH_4]^+$ indicates molecular mass of triacylglycerols (TAG) with the addition of ammonium ion as adduct, fragments' molecular mass refer to diacylglycerols (DAG) ions where Bu: butyric (C4), La: lauric (C12), P: palmitic (C16), S: stearic (C18), O: oleic (C18:1). Complete identification refers to **Table S1**.

The identification of TAG was achieved by mass spectra analysis.[1] For example, the peak number **15** was identified as 1(3)-butyryl-2-palmitoyl-1(3)-stearoyl glycerol (BuPS), where the main mass spectrum value (m/z) 684.6 corresponded to the total molecular weight of this TAG (667.1) plus the molecular weight of the ammonium fragment (18). The presence of BuPS DAG fragment ions, i.e. 1-palmitoyl-2-stearoyl-sn-glycerol [P-S]+ (m/z 579.5), 1-butyryl-2-stearoyl-sn-glycerol [Bu-S]+ (m/z 411.3), and 1-butyryl-2- palmitoyl -sn-glycerol [Bu-P]+ (m/z 383.3) also confirmed that this chromatographic peak was indeed the BuPS TAG. Similarly, peak number **24** was identified as 1(3)-palmitoyl-2-lauroyl-1(3)-oleoyl glycerol (P-La-O) as its molecular weight is 777.2 and in addition with ammonium adduct corresponds to the main m/z spectra 794.7. It is worth noticing that the intensity of the fragment ions was not very strong, in some cases less than 10% of main m/z intensity. Thus, we find the similar spectra profiles in the work of Zhou et al.[2] as particularly useful. Moreover, the peak number 30 was unambiguously identified as tripalmitoyl glycerol (PPP) by comparing its retention time with that of the TAG mixture standard.

Table S1. Peak identification according to TAG molecular mass and its DAG fragments.

Peak No	RT (min)	TAG Structure	$[M+NH4]^+$	$[DAG]^+$ fragments (m/z)		
1	2.8	Bu-Co-P	516.4	$[Bu-Co]^+$ 243.2	$[Co-P]^+$ 411.3	$[Bu-P]^+$ 383.3
2	3.2	Bu-C-M	544.5	$[Bu-M]^+$ 355.3	$[M-C]^+$ 439.4	$[Bu-C]^+$ 299.2
3	3.4	n/i	750.5	-	-	-
4	3.8	Bu-C-P	572.5	$[Bu-C]^+$ 299.2	$[C-P]^+$ 467.4	$[Bu-P]^+$ 383.3
5	4.4	Bu-La-P	600.5	$[Bu-La]^+$ 327.2	$[La-P]^+$ 495.4	$[Bu-P]^+$ 383.3
6	4.5	Bu-La-O	626.5	$[Bu-C]^+$ 299.2	$[C-O]^+$ 493.4	$[Bu-O]^+$ 309.3
7	5.2	Bu-M-P	628.5	$[Bu-M]^+$ 355.3	$[M-P]^+$ 523.5	$[Bu-P]^+$ 383.3
8	5.3	Bu-M-O	654.5	$[Bu-M]^+$ 355.3	$[M-O]^+$ 549.5	$[Bu-O]^+$ 409.3
9	5.6	Bu-P-L	680.5	$[Bu-P]^+$ 383.3	$[Bu-L]^+$ 369.6	$[P-L]^+$ 537.9
10	6.1	Co-M-P	656.6	$[Co-M]^+$ 383.3	$[M-P]^+$ 523.5	$[Co-P]^+$ 411.3
11	6.3	Bu-P-P	656.6	$[Bu-P]^+$ 383.3	$[P-P]^+$ 551.5	-
12	6.5	Bu-P-O	682.6	$[Bu-P]^+$ 383.3	$[P-O]^+$ 577.5	[Bu-O]+409.3
13	6.7	Bu-O-O	708.6	$[Bu-O]^+$ 409.3	$[O-O]^+$ 603.5	-
14	7.5	Co-P-P	684.6	$[Co-P]^+$ 411.3	$[P-P]^+$ 551.5	-
15	7.7	Bu-P-S	684.6	$[Bu-P]^+$ 383.3	$[P-S]^+$ 579.5	$[Bu-S]^+$ 411.3
16	7.9	Bu-S-O	710.6	$[Bu-S]^+$ 411.3	$[S-O]^+$ 605.6	$[Bu-O]^+$ 409.3
17	8.9	P-P-Cy	712.6	$[P-P]^+$ 551.5	$[Cy-P]^+$ 439.4	-
18	9.2	Co-S-P	712.6	$[Co-S]^+$ 439.4	$[P-S]^+$ 579.5	$[Co-P]^+$ 411.3
19	9.5	P-Cy-O	738.7	$[Cy-P]^+$ 439.4	$[Cy-O]^+$ 465.4	$[P-O]^+$577.5
20	11.0	P-P-C	740.7	$[P-P]^+$ 551.5	$[P-C]^+$ 467.4	-
21	11.4	P-C-O	766.7	$[P-C]^+$ 467.4	$[P-O]^+$ 577.5	$[C-O]^+$ 493.4
22	11.8	C-O-O	792.7	$[C-O]^+$ 493.4	$[O-O]^+$ 603.5	-
23	13.7	La-P-P	768.7	$[La-P]^+$ 495.4	$[P-P]^+$ 551.5	-
24	14.2	P-La-O	794.7	$[La-P]^+$ 495.4	$[P-O]^+$ 577.5	$[La-O]^+$ 521.5
25	14.7	P-M-L	820.7	$[M-L]^+$ 521.5	$[P-L]^+$ 575.5	$[M-P]^+$ 523.5
26	17.1	M-P-P	796.7	$[M-P]^+$ 523.5	$[P-P]^+$ 551.5	-
27	17.7	P-M-O	822.7	$[M-P]^+$ 523.5	$[P-O]^+$ 577.5	$[M-O]^+$ 549.5
28	18.4	O-M-O	848.7	$[M-O]^+$549.5	$[O-O]^+$ 603.5	-
29	19.4	O-P-L	874.7	$[P-O]^+$ 577.5	$[P-L]^+$ 575.5	$[O-L]^+$ 601.5
30	21.6	P-P-P	824.7	$[P-P]^+$ 551.5	-	-
31	22.4	O-P-P	850.7	$[P-P]^+$ 551.5	$[P-O]^+$ 577.5	-
32	23.2	P-O-O	876.8	$[P-O]^+$ 577.5	$[O-O]^+$ 603.5	-
33	24.2	O-O-O	902.7	$[O-O]^+$ 603.5	-	-
34	27.3	P-P-S	852.8	$[P-P]^+$ 551.5	$[P-S]^+$ 579.5	-
35	28.4	S-P-O	878.8	$[P-S]^+$ 579.5	$[P-O]^+$ 577.5	-
36	29.6	O-O-S	904.8	$[O-O]^+$ 603.5	$[S-O]^+$ 605.6	-
37	34.8	S-P-S	880.8	$[P-S]^+$ 579.5	$[S-S]^+$ 607.6	-
38	36.3	S-S-O	906.8	$[S-S]^+$ 607.6	$[S-O]^+$ 605.6	-

RT: retention time; TAG: triacyclglycerols; DAG: diacylglycerols; $[M+NH4]^+$: molecular mass of TAG + ammonium ion; Bu: butyric (C4), Co: caproic (C6), Cy: caprylic (C8), C: capric (C10), La: lauric (C12), M: myristic (C14), P: palmitic (C16), S: stearic (C18), O: oleic (C18:1), L: linoleic (C18:2) fatty acid.

2. Small and Wide-Angle X-ray Scattering Data

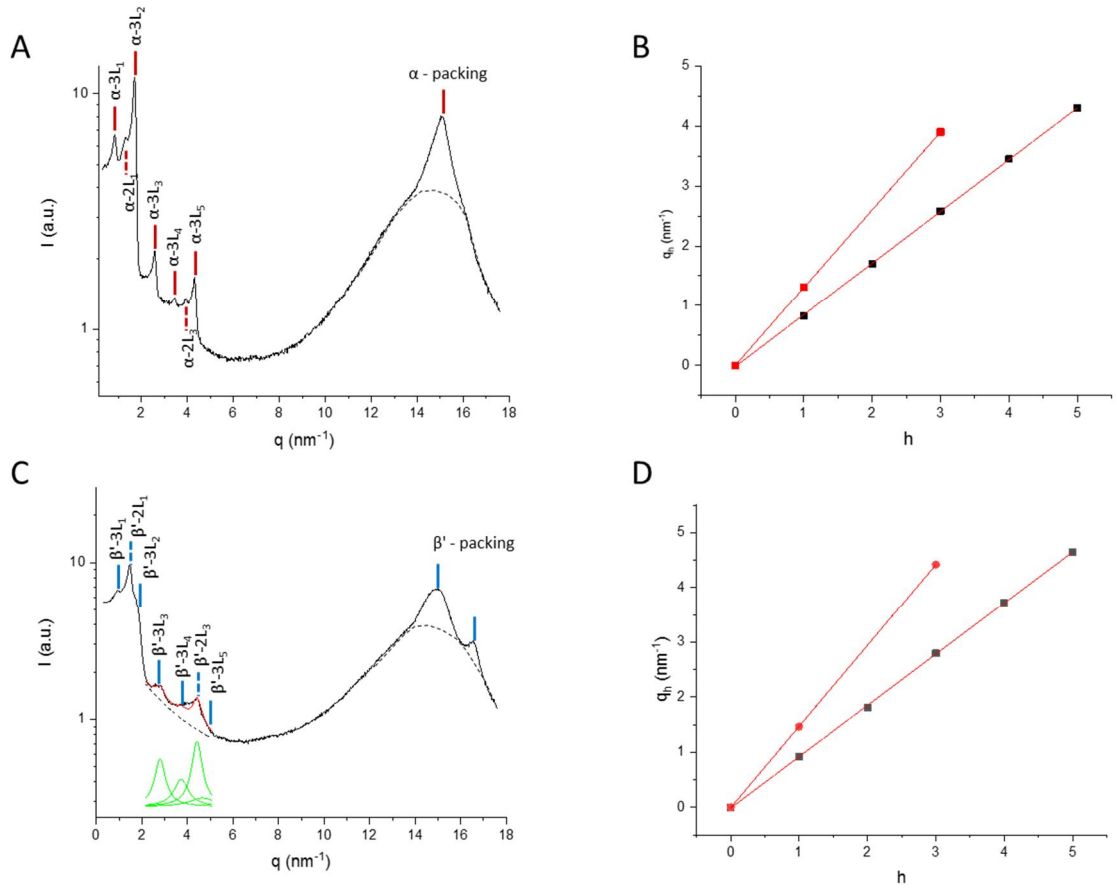

Figure S2. BMF diffraction patterns at -10 °C and indexing. A) Small- and wide-angle X-ray scattering of two co-existing α-polymorphs. B) From indexing of all recorded orders follows d = 48.4 Å for the 2L-form and d = 72.8 Å for the 3L-form. C) Small- and wide-angle X-ray scattering of two co-existing β'-polymorphs. D) From indexing of all recorded orders follows d = 42.6 Å for the 2L-form and d = 67.4 Å for the 3L-form.

Data analysis: As described in the Materials and Methods all analysed pattern were transmission corrected and the scattering contribution of the capillary was subtracted. All peaks were then fitted with Lorentz distribution and additionally fitting the diffuse scattering contributions with second degree polynomials (see dashed lines in Fig. S2). For the 2L-phases the first three orders were recorded, while for the 3L-pahse we were able to record the fits five order reflections. Most critical were the fits of the 4th and 5th order reflections in the β'-3L phase (see Lorentz fits in Fig. S2 C – green lines). In order to understand the influence of uncertainties of F_4 and F_5 onto the resulting EDP, further evaluations were carried out (cf. Fig. 3S). All resulting amplitudes together with their phases are summarised in Tables 2S and 3S.

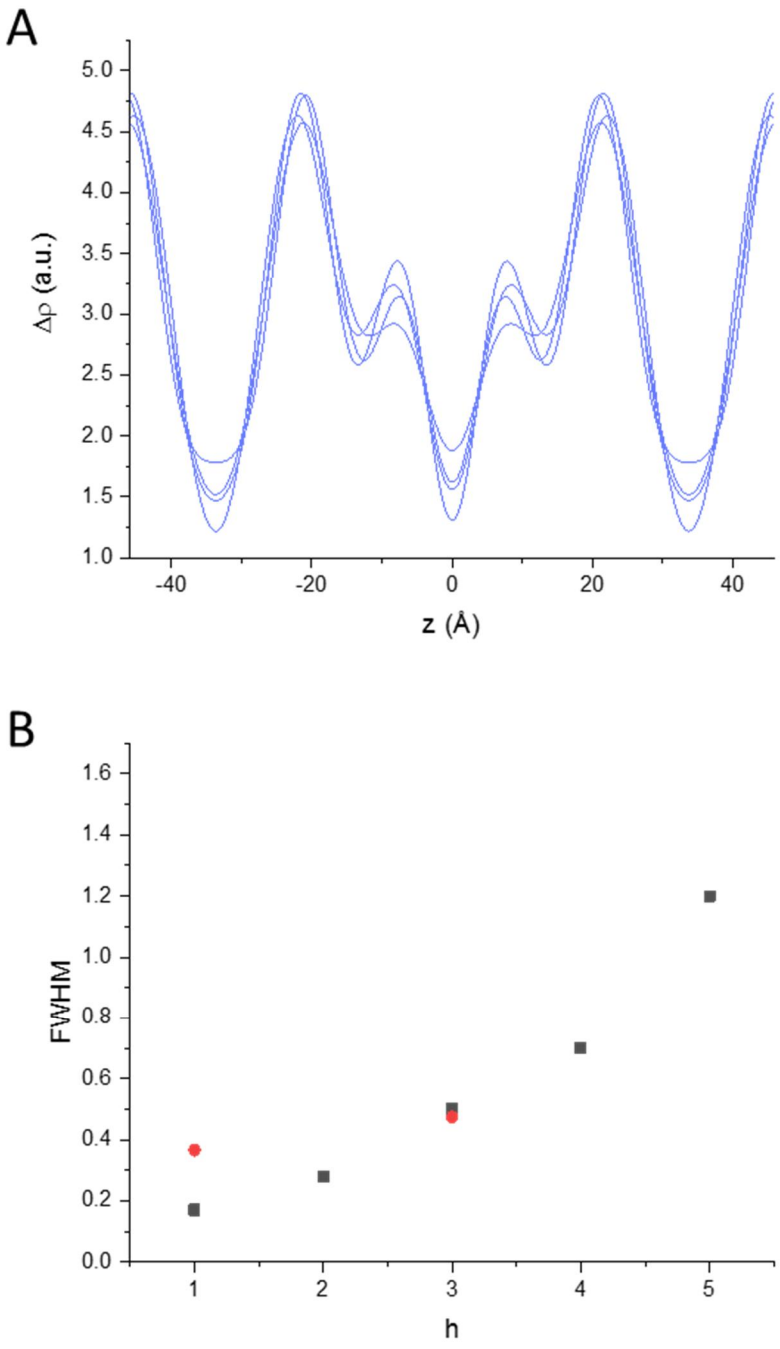

Figure S3. Analysing the error of glycerol backbone positioning in the EDPs of the β'-3L phase at -10°C. As seen in the diffraction pattern in the small angle regime (Figure S3 C) the fourth and fifth order Bragg-reflections of the β'-3L phase are not well resolved, but overlap with the third order of the β'-2L phase. A) Thus the fourth and forth order amplitudes, F_h, were varied from 0.3 to 0.6 and 0.25 to 0.5, respectively. From the resulting electron diffraction pattern, we get **the bilayer thickness, d_S, to vary from 41.8 to 44.2 Å**. B) Note, to reduce the fitting uncertainties a constraint was employed onto the FWHM as a function of diffraction order, *h*. Satisfying the lattice disorder of second kind only monotonous increasing *FWHM(h)* were allowed.

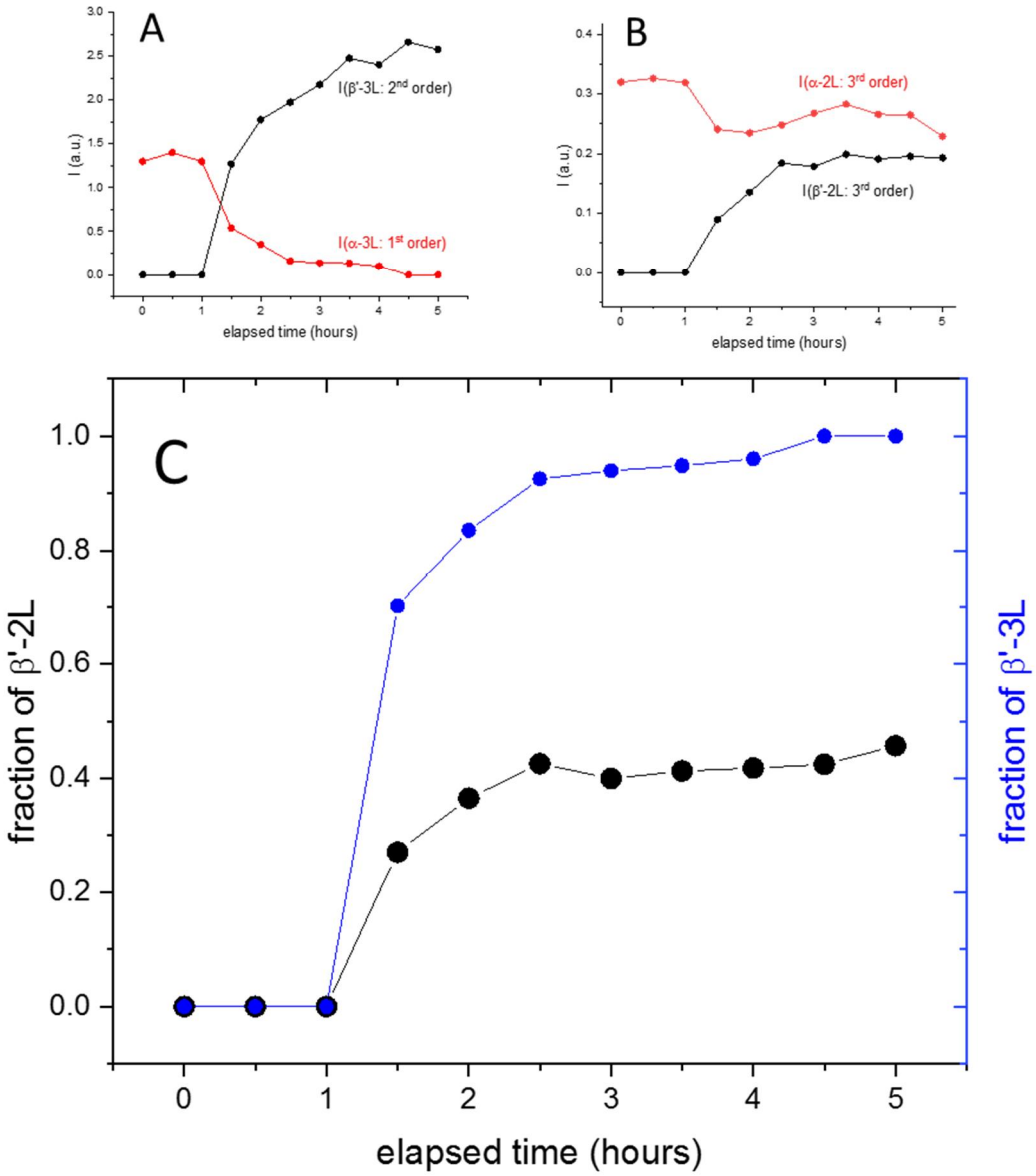

Figure S4. The α-3L to β' 3L and α-2L to β' 2L and transitions. A) Intensity of the 1st order diffraction peak of the α-3L phase (red circles) and 2nd order diffraction peak of the β'-3L phase (black circles) as function of elapsed time. B) Intensity of the 3rd order diffraction peak of the α-2L phase (red circles) and 3rd order diffraction peak of the β'-2L phase (black circles) as function of elapsed time. C) Fraction of the β'-2L (black circles) and β'-3L phase (blue circles) as function of elapsed time. The fractions were calculated as I(β')/[I(α)+I(β')]. Note, we have chosen the strongest reflections of each phase, where possible, and only weaker reflections, when they were nicely isolated in the diffraction pattern. All intensity data refer to the diffraction pattern presented in Figure 4.

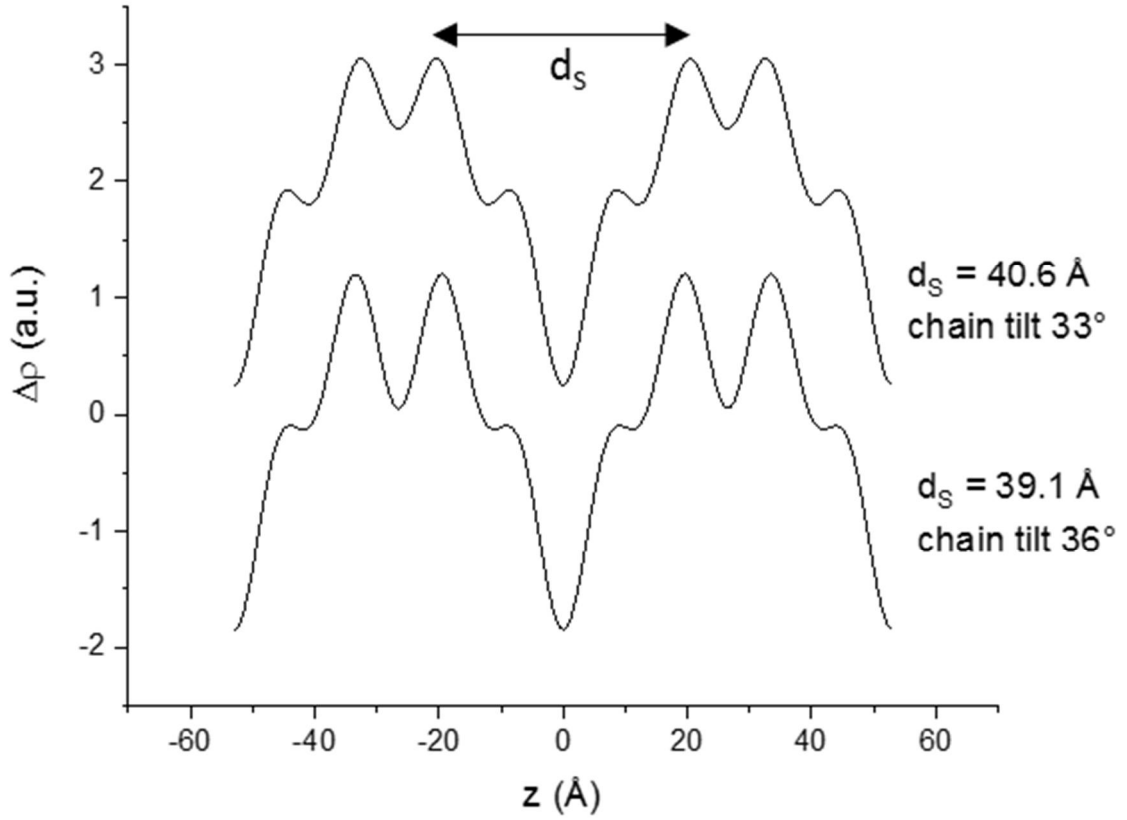

Figure S5. Simulation of the electron density profile (EDP) of the 3L-β phase. To obtain a first idea about the possible electron density profile of the observed 3L-β phase (d = 53 Å), two assumptions were made. First, we assumed the chain tilt in the bilayer region to be comparable to literature data,[3] that is, ideally a chain tilt of 36° is assumed (see bottom EDP). In a second simulation, a slightly looser chain packing with 33° tilt was assumed (upper EDP). The second important assumption was to expect in the bilayer region mainly longer saturated chains (palmitic and stearic fatty acids) as we observed for the 2L-α and 2L-β' polymorphs, i.e., d_S = d(2L-α) cos(36°) and d_S = d(2L-α) cos(33°), respectively. Finally, EDPs were simulated with variation of the amplitudes F_2, F_3 and F_4, until the predicted d_S-value was obtained. Noteworthy, $\boldsymbol{d_U}$ **with values in the range of 12 to 14 Å is rather small** (note, $d = d_S + d_U$). Note, best values for F_2, F_3 and F_4 were -0.45, +0.05 and -0.45 (chain tilt 36°) and -0.25, +0.10 and -0.40 (chain tilt 33°), respectively. Note F_1 was fixed -1.00.

Table S2. Structural parameters of the 2L-α, 3L-α, 2L-β' and 3L-β' polymorphs at -10 °C.

	2L-α[a]	**3L-α**[b]	**2L-β'**[c]	**3L-β'**[d]
h	F_h	F_h	F_h	F_h
1	-1.00	-0.24	-1.00	-0.18
2	-	-1.00	-	-1.00
3	-0.54	+0.37	-0.59	+0.60
4	-	-0.16	-	-0.61
5	-	-0.60	-	-0.50

[a] d = 48.4 Å; [b] d = 72.8 Å; [c] d = 42.6 Å;[d] d = 67.4 Å.

Table S3. Amplitudes of the SOS α-3L and γ-3L phases compared to the α-3L ones of BMF.

	3L-α (SOS)[a]	**3L-γ (SOS)**[b]	**3L-α (BMF)**[c]
h	F_h	F_h	F_h
1	-0.84	-0.07	-0.24
2	-1.00	-1.00	-1.00
3	+0.12	+0.41	+0.37
4	-0.43	-0.11	-0.16
5	-	-0.69	-0.60

[a] d = 55.6 Å; [b] d = 74.8 Å; [c] d = 72.8 Å.

Remark: Although the recorded diffraction pattern in the wide-angle region of the 3L-α polymorph of BMF clearly displays the chain packing of a α-phase (perfect hexagonal chain packing with free chain-rotation), the long spacings and corresponding amplitudes, F_h, are strikingly similar to the 3L-γ polymorph of SOS.[3] In contrast, the electron density profile of the 3L-α polymorph of SOS is clearly different to the 3L-α polymorph of BMF.

References

(1) Zeb, A.; Murkovic, M. Analysis of Triacylglycerols in Refined Edible Oils by Isocratic HPLC-ESI-MS. *Eur. J. Lipid Sci. Technol.* **2010**, *112*, 844–851. https://doi.org/10.1002/ejlt.201000064.

(2) Zhou, Q.; Gao, B.; Zhang, X.; Xu, Y.; Shi, H.; Yu, L. Chemical Profiling of Triacylglycerols and Diacylglycerols in Cow Milk Fat by Ultra-Performance Convergence Chromatography Combined with a Quadrupole Time-of-Flight Mass Spectrometry. *Food Chem.* **2014**, *143*, 199–204. https://doi.org/10.1016/j.foodchem.2013.07.114.

(3) Mykhaylyk, O. O.; Hamley, I. W. The Packing of Triacylglycerols from SAXS Measurements: Application to the Structure of 1,3-Distearoyl-2-Oleoyl-Sn-Glycerol Crystal Phases. *J. Phys. Chem. B* **2004**, *108* (23), 8069–8083. https://doi.org/10.1021/jp0379704.